Electronic supplementary information

MnO_2-Coated Porous Pt@CeO_2 Core-Shell Nanostructures for Photoacoustic Imaging-Guided Tri-modal Cancer Therapy

Qing Xu,[‡a] Danyang Li,[‡a] Haijun Zhou,[a] Biaoqi Chen,[b,c] Junlei Wang,[a] Shi-Bin Wang,[b,c] Aizheng Chen[b,c] and Nina Jiang*[a,b,c]

[a] *College of Chemical Engineering, Huaqiao University, Xiamen 361021, China*

[b] *Institute of Biomaterials and Tissue Engineering, Huaqiao University, Xiamen 361021, P. R. China*

[c] *Fujian Provincial Key Laboratory of Biochemical Technology (Huaqiao University), Xiamen 361021, P. R. China*

‡ *These authors contributed equally to this work.*

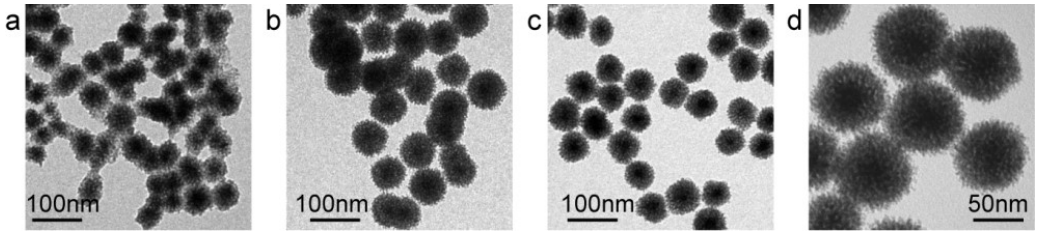

Fig. S1 Effects of the amount of $Ce(NO_3)_3$ on $Pt@CeO_2$ nanostructures. (a–c) TEM images of $Pt@CeO_2$ nanostructures synthesized with 0.04 mL, 0.1 mL, 0.12 mL of $Ce(NO_3)_3$ (0.04 M), respectively. (d) High-magnification TEM image of $Pt@CeO_2$ nanostructures synthesized with 0.04 mL of $Ce(NO_3)_3$ (0.04 M).

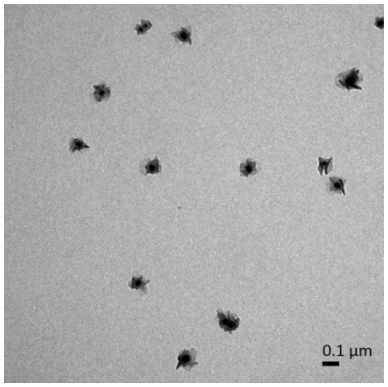

Fig. S2 Low-magnification TEM image of $Pt@CeO_2@MnO_2$ nanostructures.

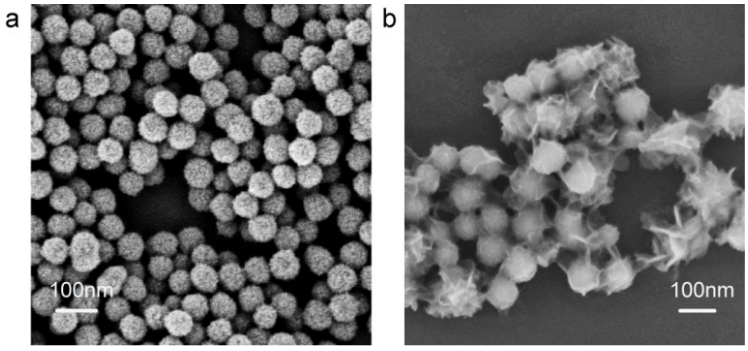

Fig. S3 SEM images of (a) $Pt@CeO_2$ and (b) $Pt@CeO_2@MnO_2$ nanostructures.

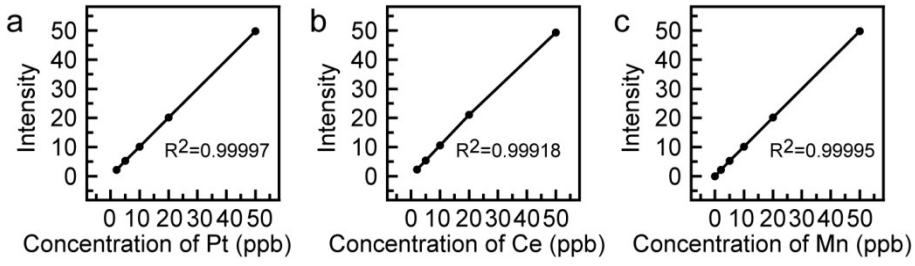

Fig. S4 Linear calibration relationships between the emission intensity and the atomic mass concentration for (a) Pt, (b) Ce and (c) Mn in the ICP-MS measurements.

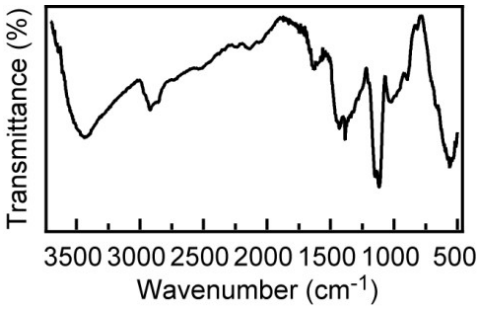

Fig. S5 Fourier-transform IR (FTIR) spectra of PEG-stabilized $Pt@CeO_2@MnO_2$ nanostructures.

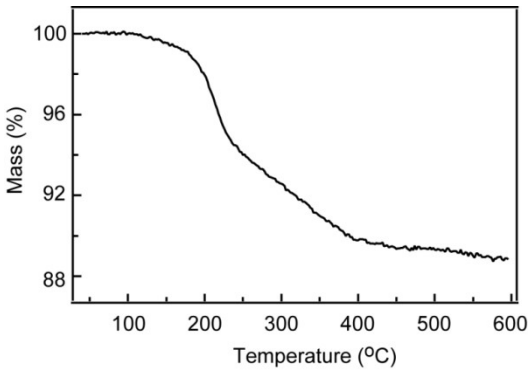

Fig. S6 Thermogravimetric curve of PEG-stabilized $Pt@CeO_2@MnO_2$ nanostructures.

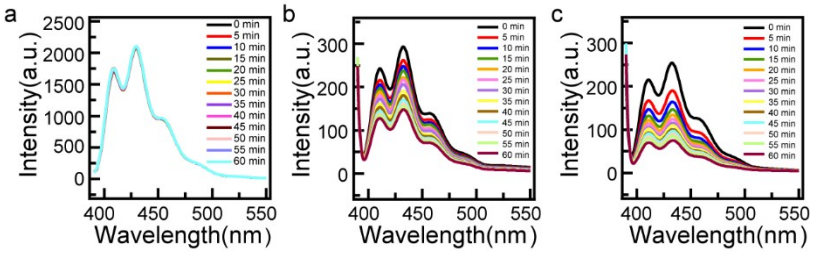

Fig. S7 Time-dependent fluorescence spectra of ABDA reacting with $^1O_2$ produced by (a) Pt NP, (b) $Pt@CeO_2$ and (c) $Pt@CeO_2@MnO_2$ nanostructure samples under 808-nm laser irradiation.

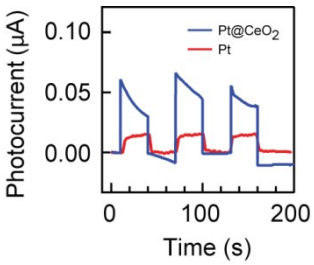

Fig. S8 Transient photocurrent–time curves for $Pt@CeO_2$ nanostructures and Pt NPs recorded under the 808-nm laser irradiation.

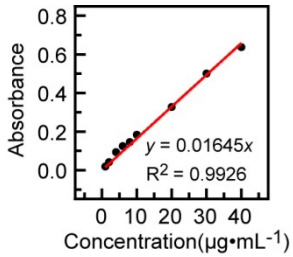

Fig. S9 Linear calibration relationship between the absorbance at 480 nm and the concentration of doxorubicin (DOX).

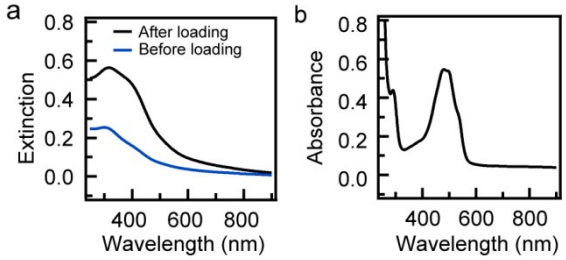

Fig. S10 (a) Extinction spectra of $Pt@CeO_2@MnO_2$ nanostructures before and after DOX loading. (b) Absorption spectra of the aqueous DOX solution.

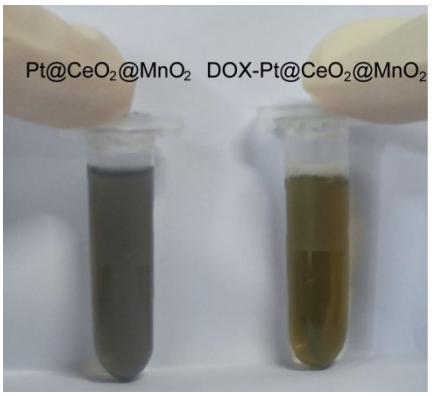

Fig. S11 Photographs of $Pt@CeO_2@MnO_2$ and DOX-$Pt@CeO_2@MnO_2$ nanostructure solutions.

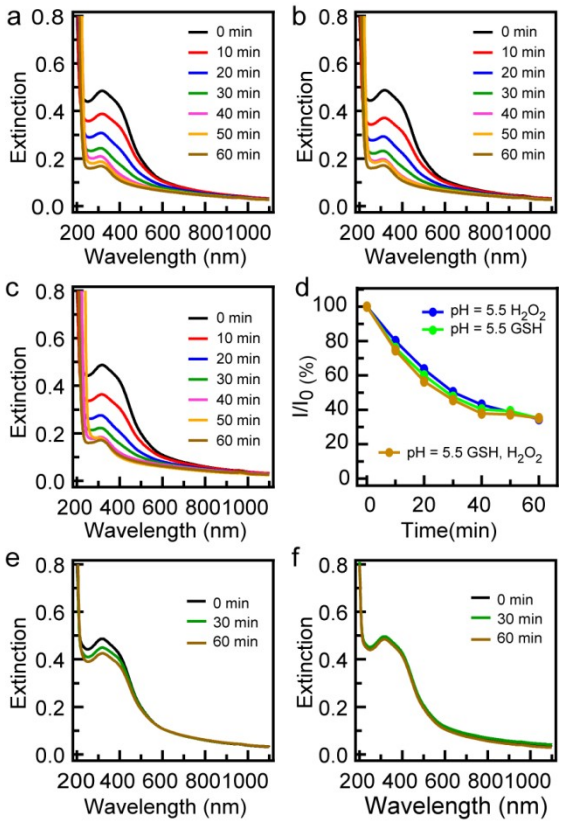

Fig. S12 Tumor microenvironment (TME)-responsive behaviours of DOX-Pt@CeO_2@MnO_2 nanostructures. (a–c) Extinction spectra of DOX-Pt@CeO_2@MnO_2 nanostructures in pH = 5.5 PBS solutions containing (a) H_2O_2, (b) glutathione (GSH) and (c) H_2O_2 and GSH for different times. (d) Variations of the absorption peaks at 314 nm shown in (a–c) with the time. (e, f) Extinction spectra of DOX-Pt@CeO_2@MnO_2 nanostructures in pH =7.4 PBS solutions with and without H_2O_2 and GSH.

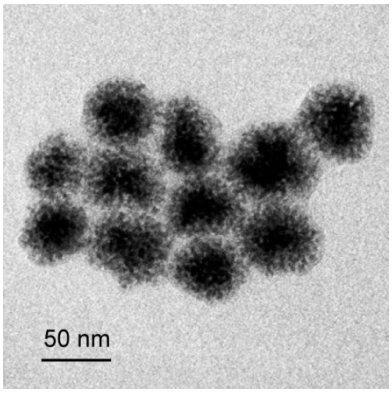

Fig. S13 TEM images of Pt@CeO_2@MnO_2 nanostructures treated by PBS solution (pH = 5.5) with GSH and H_2O_2.

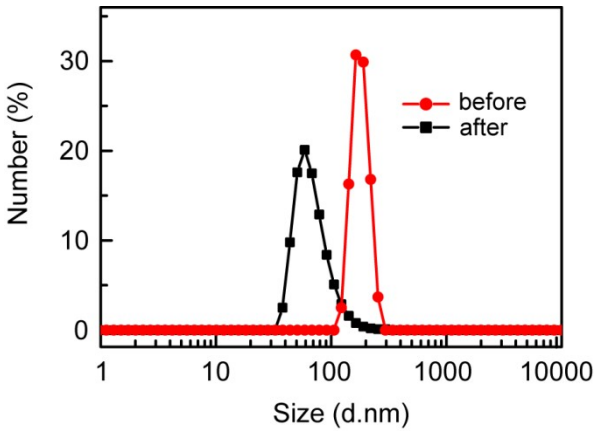

Fig. S14 Dynamic light scattering data of Pt@CeO_2@MnO_2 nanostructures before and after treated by pH = 5.5 solution with GSH and H_2O_2.

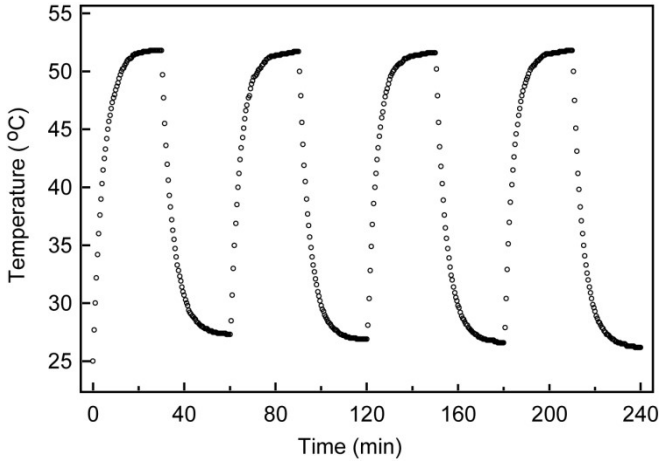

Fig. S15 Temperature change curves of the DOX-Pt@CeO_2@MnO_2 nanostructures in water (1 mL, 200 μg mL^{-1}) with four temperature cycles under an 808-nm laser irradiation at 1 W.

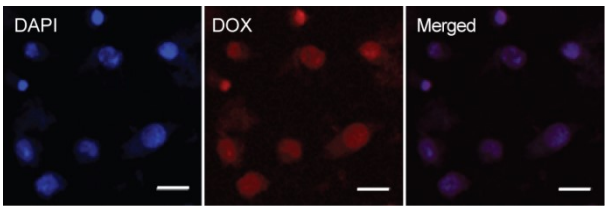

Fig. S16 Confocal fluorescence microscope images of tumor cells incubated with DOX-Pt@CeO_2@MnO_2 after 8 h. Scale bar: 20 μm.

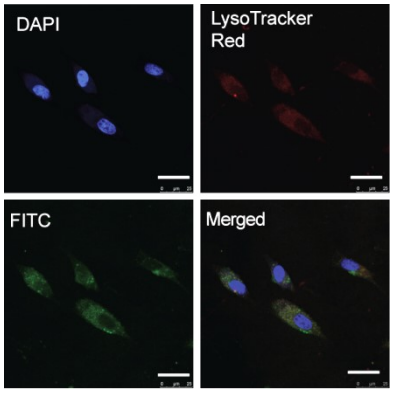

Fig. S17 Confocal fluorescence microscope images of tumor cells incubated with DOX-Pt@CeO_2@MnO_2 for 4 h. Scale bar: 25 μm.

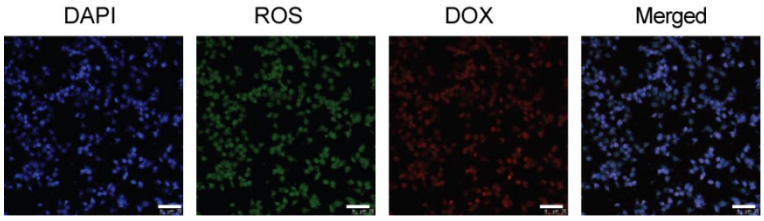

Fig. S18 Confocal fluorescence microscope images of tumor cells which are incubated with DOX-Pt@CeO_2@MnO_2 and DCFH-DA probe for 4 h and then treated with 808-nm laser irradiation. Scale bar: 75 μm.